Inorganica Chimica Acta 395 (2013) 124–134

Contents lists available at SciVerse ScienceDirect

Inorganica Chimica Acta

journal homepage: www.elsevier.com/locate/ica

Iron(III) complexes of ethylenediamine derivatives of aminophenol ligands as models for enzyme–substrate adducts of catechol dioxygenases

Touraj Karimpour [a], Elham Safaei [a,*], Andrzej Wojtczak [b], Zvonko Jagličić [c], Anna Kozakiewicz [b]

[a] Institute for Advanced Studies in Basic Sciences (IASBS), 45195 Zanjan, Iran
[b] Nicolaus Copernicus University, Department of Chemistry, 87-100 Torun, Poland
[c] Institute of Mathematics, Physics and Mechanics & Faculty of Civil and Geodetic Engineering, University of Ljubljana, Jadranska 19. SI-1000 Ljubljana, Slovenia

ARTICLE INFO

Article history:
Received 11 June 2012
Received in revised form 19 September 2012
Accepted 9 October 2012
Available online 2 November 2012

Keywords:
Catechol dioxygenase
Non-heme
Model complexes
Intradiol-cleaving
Extradiol-cleaving
Mononuclear iron(III) complexes

ABSTRACT

In the present work, six *N*,*N*′-dimethylethylenediamine derivatives of substituted aminophenol ligands (H_2L^{NEX}, X: C, B, M, BM, Bu and OB) were synthesized by a convenient, green procedure. The mentioned ligands were characterized by ^{1}H NMR and IR spectroscopies. iron complexes (FeL^{NEX}, X: C, B, M, BM, Bu and OB) of mentioned ligands, have been synthesized and characterized by IR, UV–Vis, elemental analysis, single crystal X-ray diffraction, magnetic susceptibility studies and cyclic voltammetry techniques. X-ray structure analysis has revealed that Fe(III) centers were surrounded by two phenolates, two amine nitrogens and two oxygen atoms of acetylacetonate ligand similar to the proposed catechol-bound intermediate for catechol dioxygenase. The variable temperature magnetic susceptibility indicates paramagnetic iron(III) in monomer complexes. All complexes undergo a metal-centered reduction, and a ligand-centered oxidation.

1. Introduction

Catechol dioxygenases are mononuclear non-heme iron enzymes which catalyze the oxidative cleavage of toxic environmental catechol substrates [1–3]. Soil bacteria containing these enzymes provide their carbon and energy through aerobic biodegradation of aromatic hydrocarbons [4–6] with concomitant insertion of molecular oxygen into the aromatic ring of the substrate resulting in production of aliphatic acids.

Catechol dioxygenases subdivided into two classes on the basis of the site of aromatic ring cleavage [7]: The intradiol catechol dioxygenases, utilize mononuclear iron(III) centers to catalyze the oxidative cleavage of the carbon–carbon bond between the two phenolic hydroxyl groups, while the extradiol-type enzymes contain a non-heme iron(III) co-factor, cleave the adjacent carbon–carbon bond. (Scheme1).

Many of the reported mimics of the catechol dioxygenases have focused on the tetradentate all-nitrogen donor ligands, [8–12] and complexes with phenolato groups as structural and functional models for the catecholate-iron(III) form of catechol dioxygenases [13–20].

Herein, we describe: (1) Synthesis of new tetradentate aminophenol ligands containing substituted phenol and *N*,*N*′-dimethylethylenediamine units (Scheme 2). (2) Synthesis of the acetylacetonato iron(III) complexes of mentioned ligands as models for mononuclear non-heme iron intermediates. (3) Significance of Lewis acidity of iron(III) centers for the structural and electronic properties of dioxygenase–substrate adduct models.

2. Experimental

2.1. Materials and physical measurements

Reagents or analytical grade materials were obtained from commercial suppliers and used without further purification, except those for electrochemical measurements. Elemental analyses (C. H. N.) were performed by the Isfahan University of Technology. Fourier transform infrared spectroscopy on KBr pellets was performed on a FT IR Bruker Vector 22 instrument. NMR measurements were performed on a Bruker 400 instrument. UV–Vis absorbance digitized spectra were collected using a Ultrospec 3100 Pro spectrophotometer.

Magnetic susceptibility were measured from powder samples of solid material in the temperature range 2–300 K by using a SQUID susceptometer (Quantum Design MPMS-XL-5) in a magnetic field of 1000 Oe.

Voltammetric measurements were made with a computer controlled electrochemical system (ECO Chemie, Ultrecht, The Netherlands) equipped with a PGSTA 30 model and driven by GPES

---

* Corresponding author. Tel.: +98 241 4153200; fax: +98 241 4153232.
E-mail address: safaei@iasbs.ac.ir (E. Safaei).

0020-1693/$ - see front matter © 2012 Elsevier B.V. All rights reserved.
http://dx.doi.org/10.1016/j.ica.2012.10.015

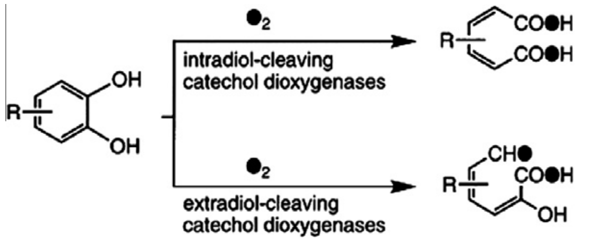

Scheme 1. Scheme of cleavage by intradiol and extradiol dioxygenases [7].

(ECO Chemie). A glassy carbon electrode with a surface area of 0.035 cm^2 was used as a working electrode and a platinum wire served as the counter electrode. The reference electrode was an Ag wire as the quasi reference electrode. Ferrocene was added as an internal standard after completion of a set of experiments, and potentials are referenced vs. the ferrocenium/ferrocene couple (Fc^+/Fc).

Crystals of the FeL^{NEC}, FeL^{NEB}, FeL^{NEM}, FeL^{NEBM}, FeL^{NEBu} and FeL^{NEOB} complexes suitable for the X-ray diffraction experiment were obtained from the $EtOH–CH_2Cl_2$ solutions. The X-ray data were collected with an Oxford Sapphire CCD diffractometer using Mo Kα radiation $\lambda = 0.71073$ Å, at 293(2) K, by $\omega–2\theta$ method. All structures have been solved by direct methods and refined with the full-matrix least-squares method on F2 with the use of SHELX97 [21] program package. The numerical absorption corrections were applied (RED171 package of programs [22] Oxford Diffraction, 2000). No extinction correction was applied. For all structures, positions of hydrogen atom were calculated from geometry, and hydrogen atoms were constrained in the refinement.

2.2. Preparations

2.2.1. Synthesis of ligands

Ligands were synthesized according to the modified literature procedure [23,24].

A solution of phenol (24.00 mmol), *N,N′*-dimethylethylenediamine (1.06 g, 12 mmol), and 37% aqueous formaldehyde (4.31 mL, 58 mmol) was refluxed for 48 h. Upon cooling, a large quantity of beige solid was formed. The solvent was decanted, and the remaining solid residue was washed with cold methanol to give a pure, white powder.

2.2.1.1. Synthesis of H_2L^{NEC} *[6,6′-((ethane-1,2-diylbis(methylazanediyl))bis(methylene))bis(2,4-dichlorophenol)].* (4.00 g, 76% yield). ^1H NMR (400 MHz, $CDCl_3$, 298 K): δ 2.345 (s, 6H); 2.734 (s, 4H); 3.721 (s, 4H); 6.895 (d, 2H); 7.294 (d, 2H); 10.884 (br, 2H). IR(cm^{-1}): 3421 (OH); 2817 (C–H); 1459 (C═C, phenyl ring). m.p. 167–168 °C.

2.2.1.2. Synthesis of H_2L^{NEB} *[6,6′-((ethane-1,2 diylbis(methylazanediyl))bis(methylene)) bis(2,4-dibromophenol)].* (5.20 g, 70 yield). ^1H NMR(400 MHz, $CDCl_3$, 298 K): δ 2.331 (s, 6H); 2.723 (s, 4H); 3.707 (s, 4H); 7.064 (d, 2H); 7.579 (d, 2H); 10.964 (br, 2H). IR(cm^{-1}): 3435 (OH); 2793 (C–H); 1455 (C═C, phenyl ring). m.p. 159–160 °C.

2.2.1.3. Synthesis of H_2L^{NEM} *[6,6′-((ethane-1,2-diylbis(methylazanediyl))bis(methylene)) bis(2,4-dimethylphenol)].* (3.20 g, 75% yield). ^1H NMR(400 MHz, $CDCl_3$, 298 K): δ 2.216 (s, 6H); 2.241(s, 6H); 2.292 (s, 6H); 2.684 (s, 4H); 3.660 (s, 4H); 6.635 (d, 2H); 6.889 (d, 2H); 10.626 (br, 2H). IR(cm^{-1}): 3451(OH); 2813 (C–H); 1477 (C═C, phenyl ring). m.p. 131–132 °C.

2.2.1.4. Synthesis of H_2L^{NEBM} *[6,6′-((ethane-1,2-diylbis(methylazanediyl))bis(methylene)) bis(2-(tert-butyl)-4-methylphenol)].* (4.30 g, 81% yield). ^1H NMR(400 MHz, $CDCl_3$, 298 K): δ 1.443 (s, 18H); 2.288 (s, 12H); 2.656 (s, 4H); 3.677 (s, 4H); 6.679 (s, 2H); 7.040 (s, 2H); 10.666 (br, 2H). IR(cm^{-1}): 3414 (OH); 2959 (C–H); 1459 (C═C, phenyl ring). m.p. 128–130 °C.

2.2.1.5. Synthesis of H_2L^{NEBu} *[6,6′-((ethane-1,2-diylbis(methylazanediyl))bis(methylene)) bis(2,4-di-tert-butylphenol)].* (4.50 g, 71% yield). ^1H NMR(400 MHz, $CDCl_3$, 298 K): δ 1.317 (d, 18H); 1.467 (d, 18H); 2.292 (s, 6H); 2.666 (s, 4H); 3.695 (s, 4H); 6.834 (d, 2H); 7.234 (d, 2H); 10.747 (br, 2H). IR(cm^{-1}): 3448 (OH); 2959 (C–H); 1472 (C═C, phenyl ring). m.p. 162–163 °C.

2.2.1.6. Synthesis of H_2L^{NEOB} *[6,6′-((ethane-1,2-diylbis(methylazanediyl))bis(methylene)) bis(2-(tert-butyl)-4-methoxyphenol)].* (5.00 g,

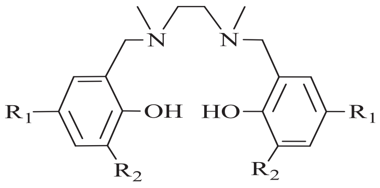

H_2L^{NEX}	R_1	R_2
H_2L^{NEC}	Cl	Cl
H_2L^{NEB}	Br	Br
H_2L^{NEM}	Me	Me
H_2L^{NEMB}	^tBu	Me
H_2L^{NEBM}	Me	^tBu
H_2L^{NEBu}	^tBu	^tBu
H_2L^{NEOB}	OMe	^tBu

Scheme 2. Amine bis(phenolate) ligands used in this study.

88% yield). ^1H NMR(400 MHz, $CDCl_3$, 298 K): δ 1.417 (s, 18H); 2.274 (s, 6H); 2.633 (s, 4H); 3.663 (s, 4H); 3.771 (s, 6H); 6.418 (d, 2H); 6.827 (d, 2H); 10.384 (br, 2H). IR(cm^{-1}): 3414 (OH); 2957 (C–H); 1460 (C=C, phenyl ring). m.p. 127–128 °C.

2.2.2. Synthesis of complexes

Triethylamine (0.20 g, 2.00 mmol) was added to a solution of H_2L^{NEX} (1.00 mmol) in ethanol. $Fe(acac)_3$ (0.35 g, 1.00 mmol) was added to this solution and the resulting mixture was refluxed for 2 h, resulting in an intense dark red for FeL^{NEC} and FeL^{NEB} and purple solution for other complexes. Solvent was removed and the solid material crystallized in 1:1 dichloromethane and ethanol mixture.

2.2.2.1. Synthesis of FeL^{NEC}. Yield: 0.46 g (78%). *Anal.* Calc. for $C_{23}H_{25}Cl_4FeN_2O_4$ (591.11 g/mol) C, 46.77; H, 4.05; N, 4.65%. Found: C, 46.65; H, 4.43; N, 4.73%. IR (KBr, cm^{-1}): 3447, 2895, 1580, 1524, 1456, 1363, 1317, 1271, 1217, 1173, 1056, 1019, 928, 866, 759, 662, 575, 465, UV–Vis in CH_2Cl_2: λ_{max}, nm (ε, $M^{-1}\,cm^{-1}$): 290 (25 149), 500 (7714).

2.2.2.2. Synthesis of FeL^{NEB}. Yield: 0.56 g (73%). *Anal.* Calc. for $C_{23}H_{25}Br_4FeN_2O_4$ (768.92 g/mol): C, 36.01; H, 3.27; N, 3.72%. Found: C, 35.88; H, 3.40; N, 3.64%. IR (KBr, cm^{-1}): 3446, 2866, 1574, 1523, 1451, 1360, 1316, 1275, 1154, 1018, 927, 855, 712, 562, 479, 427, UV–Vis in CH_2Cl_2: λ_{max}, nm (ε, $M^{-1}\,cm^{-1}$): 289 (22 521), 518 (5128).

2.2.2.3. Synthesis of FeL^{NEM}. Yield: 0.36 g (70%). *Anal.* Calc. for $C_{27}H_{37}FeN_2O_4$ (509.44 g/mol): C, 63.53; H, 7.02; N, 5.46%. Found: C, 63.53; H, 7.50; N, 5.49%. IR (KBr, cm^{-1}): 3448, 2968, 2907, 1586, 1518, 1469, 1370, 1313, 1266, 1158, 1059, 1021, 866, 819, 744, 663, 593, 543, 506, 470. UV–Vis in CH_2Cl_2: λ_{max}, nm (ε, $M^{-1}\,cm^{-1}$): 278 (23 892), 529 (6197).

2.2.2.4. Synthesis of FeL^{NEBM}. Yield: 0.48(81%). *Anal.* Calc. for $C_{33}H_{49}FeN_2O_4$ (593.60 g/mol): C, 66.35; H, 8.13; N, 4.76%. Found: C, 66.66; H, 8.48; N, 4.71%. IR (KBr, cm^{-1}):3414, 2956, 2911, 2863, 1724, 1591, 1521, 1451, 1378, 1306, 1266, 1023, 869, 808, 709, 594, 545, UV–Vis in CH_2Cl_2: λ_{max}, nm (ε, $M^{-1}\,cm^{-1}$): 284 (11 752), 536 (3483).

2.2.2.5. Synthesis of FeL^{NEBu}. Yield: 0.46 g (68%). *Anal.* Calc. for $C_{39}H_{61}FeN_2O_4$ (677.76 g/mol): C, 69.26; H, 9.01; N, 4.18%. Found: C, 69.01; H, 9.21; N, 4.13%. IR (KBr, cm^{-1}): 3446, 2954, 2906, 2865, 1590, 1524, 1469, 1374, 1301, 1256, 1203.50, 1166, 1088, 1022, 924, 877, 837, 807, 541, 476, UV–Vis in CH_2Cl_2: λ_{max}, nm (ε, $M^{-1}\,cm^{-1}$): 280 (20 767), 541 (5278).

2.2.2.6. Synthesis of FeL^{NEOB}. Yield: 0.52(83%). *Anal.* Calc. for $C_{33}H_{49}FeN_2O_6$ (625.60 g/mol): C, 63.41; H, 7.73; N, 4.55%. Found: C, 63.25; H, 8.04; N, 4.47%. IR (KBr, cm^{-1}):3714, 3414, 2951, 2861, 1724, 1641, 1585, 1520, 1458, 1426, 1364, 1313, 1266, 1203, 1064, 1022, 927, 869, 822, 792, UV–Vis in CH_2Cl_2: λ_{max}, nm (ε, M^{-1} -cm^{-1}): 300 (15 299), 558 (5086).

3. Results and discussion

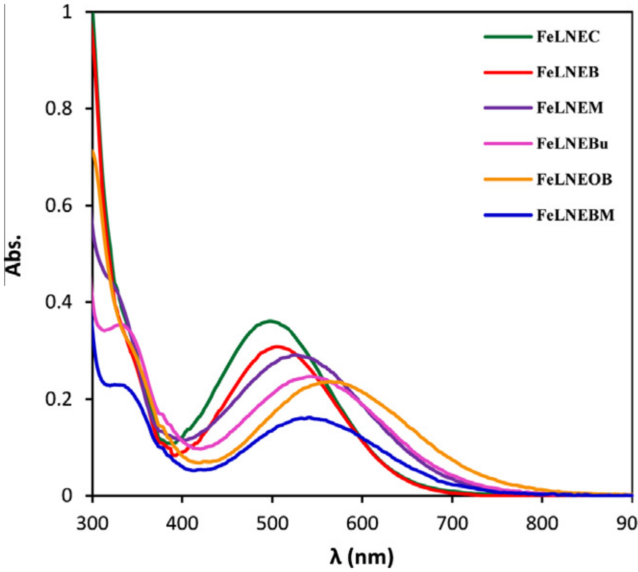

Fig. 1. Electronic absorption spectra of FeL^{NEX} (X: C, B, M, BM, Bu and OB) in (4.7×10^{-5} M) CH_2Cl_2 solution.

H_2L^{NEX}]X: C, B, M, BM, Bu and OB [, were prepared from *N,N′* dimethylethylenediamine, formaldehyde and 2,4-di-]Cl, Br, Me, ^tBu and OMe[phenol, in one step Mannich condensation. Aminophenol ligands are usually prepared in methanol solutions but we describe herein the green synthesis when water is used as the reaction medium. In fact, since aqueous formaldehyde is one of the reagents, no additional solvent is required since it is already present in the reagent solution.

The iron(III) complexes were synthesized by the following procedure (Eq. (1)).

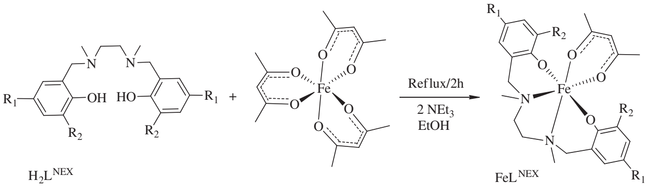

(1)

The structures and purity of complexes have been confirmed by X-ray single crystal analysis and IR spectroscopy, as well as elemental analysis. IR spectra were recorded in the region 400–4000 cm^{-1} with samples as KBr disks. In IR spectra of complexes, the strong and sharp OH stretching band of the phenols around 3300–3500 cm^{-1} for the ν_{OH} stretch of ligands were replaced by a broad band, proving the coordination of phenol groups to the metal.

The electronic absorption spectra of complexes have been measured in dichloromethane in the 200–800 nm range. In all complexes, the absorption maxima observed in the near-UV regions (below 300 nm) are caused by $\pi \rightarrow \pi*$ transitions involving the phenolate units.

The visible spectrum (between 400 and 700 nm) of FeL^{NEX} complexes showed that there are two absorption features in these spectra which are assigned to phenolate(π)-to-Fe(III)(d$\pi*$) charge transfer (LMCT) transitions (Fig. 1, Table 1).

Table 1
λ_{max} (nm) ε (($M^{-1}\,cm^{-1}$) LMCT band of complexes FeL^{NEX} (X: C, B, M, BM, Bu and OB).

FeL^{NEX}	λ_{max} (nm) (ε ($M^{-1}\,cm^{-1}$))
FeL^{NEC}	500 (7714)
FeL^{NEB}	518 (5128)
FeL^{NEM}	529 (6197)
FeL^{NEBM}	536 (3483)
FeL^{NEBU}	541 (5278)
FeL^{NEOB}	558 (5086)

Table 2
Crystallographic and structure refinement data for compounds FeL^{NEC}, FeL^{NEB} and FeL^{NEM}.

	FeL^{NEC}	FeL^{NEB}	FeL^{NEM}
Identification code	e303abs	297abs	e300abs
Formula	$C_{23}H_{27}Cl_4FeN_2O_5$	$C_{23}H_{27}Br_4FeN_2\ O_5$	$C_{27}H_{39}FeN_2O_5$
Formula weight	609.12	786.96	527.45
T (K)	293(2)	293(2)	293(2)
λ (Å)	0.71073	0.71073	0.71073
Crystal system, space group	monoclinic, $P2_1/n$	monoclinic, $P2_1/n$	monoclinic, $P2_1/n$
Unit cell dimensions			
a (Å)	8.4682(3)	8.7434(3)	8.4632(6)
b (Å)	15.1231(5)	15.1604(5)	15.2043(9)
c (Å)	21.2053(8)	21.3449(8)	21.6176(15)
α (°)	90	90	90
β (°)	92.699(3)	93.018(4)	93.473(6)
γ (°)	90	90	90
V (Å^3)	2712.65(16)	2825.42(17)	2776.6(3)
Z (Mg/m^3)	4, 1.491	4, 1.850	4, 1.262
Absorption coefficient (mm^{-1})	0.986	6.225	0.580
F(000)	1252	1540	1124
Crystal size (mm)	0.4801 × 0.2766 × 0.1140	0.4628 × 0.2180 × 0.1339	0.3095 × 0.1342 × 0.0429
θ (°)	2.35–28.37	2.34–28.36	2.31–28.51
Limiting indices	$-11 \leqslant h \leqslant 9$,	$-10 \leqslant h \leqslant 11$,	$-9 \leqslant h \leqslant 11$,
	$-18 \leqslant k \leqslant 20$,	$-20 \leqslant k \leqslant 20$,	$-20 \leqslant k \leqslant 19$,
	$-27 \leqslant l \leqslant 25$	$-18 \leqslant l \leqslant 27$	$-28 \leqslant l \leqslant 27$
Reflections collected/unique	18256/6125 [R(int) = 0.0288]	14108/5851 [R(int) = 0.0328]	18668/6320 [R(int) = 0.1293]
Completeness to θ	26.00 99.9%	24.80 94.0%	26.00 99.9%
Max./min. transmission	0.8959/0.6490	0.4895/0.1608	0.9755/0.8409
Data/restraints/parameters	6125/0/316	5851/0/316	6320/0/316
Goodness-of-fit on F^2	1.065	0.948	0.843
Final R indices [$I > 2\sigma(I)$]	$R_1 = 0.0514$, $wR_2 = 0.1587$	$R_1 = 0.0380$, $wR_2 = 0.1009$	$R_1 = 0.0653$, $wR_2 = 0.1528$
R indices (all data)	$R_1 = 0.0728$, $wR_2 = 0.1686$	$R_1 = 0.0746$, $wR_2 = 0.1079$	$R_1 = 0.2096$, $wR_2 = 0.1912$
Largest diff. peak and hole (e A^{-3})	1.593 and −0.424	1.388 and −0.594	0.787 and −0.441

Table 3
Crystallographic and structure refinement data for compounds FeL^{NEBu}, FeL^{NEBM} and FeL^{NEOB}.

	FeL^{NEBu}	FeL^{NEBM}	FeL^{NEOB}
Identification code	e302abs	e434a	e402abs
Formula	$C_{39}H_{61}Fe\ N_2\ O_4$	$C_{33}\ H_{49}\ Fe\ N_2\ O_4$	$C_{33}\ H_{49}\ Fe\ N_2\ O_6$
Formula weight	677.75	593.59	625.59
T (K)	293(2)	293(2)	293(2)
λ (Å)	0.71073	0.71073	0.71073
Crystal system, space group	Triclinic, $P\bar{1}$	Monoclinic, P21/c	Monoclinic, C2/c
Unit cell dimensions			
a (Å)	11.3161(5)	13.9901(5).	35.594(5)
b (Å)	13.6678(6)	12.4394(5)	13.8448(11)
c (Å)	14.8013(6)	18.6196(7).	14.0226(15)
α (°)	78.202(4)	90	90
β (°)	71.621(4)	96.777(4)	104.822(13)
γ (°)	68.081(4)	90	90
V (Å^3)	2005.62(15)	3217.7(2)	6680.4(13)
Z (Mg/m^3)	2, 1.122	4, 1.225	8, 1.244
Absorption coefficient (mm^{-1})	0.413	0.506	0.495
F(000)	734	1276	2680
Crystal size (mm)	0.7899 × 0.4933 × 0.3242	0.66 × 0.42 × 0.05	0.42 × 0.35 × 0.12
θ (°)	2.12–28.47	2.20–28.27	2.08–28.60
Limiting indices	$-15 \leqslant h \leqslant 14$,	$-18 \leqslant h \leqslant 18$,	$-44 \leqslant h \leqslant 47$,
	$-17 \leqslant k \leqslant 16$,	$-13 \leqslant k \leqslant 15$,	$-17 \leqslant k \leqslant 17$,
	$-16 \leqslant l \leqslant 19$	$-22 \leqslant \leqslant l \leqslant 23$	$-18 \leqslant l \leqslant 17$
Reflections collected/unique	13792/8822 [R(int) = 0.0368]	21397/7055 [R(int) = 0.0500]	22779/7706 [R(int) = 0.0813]
Completeness to θ	25.00 99.8%	25.00 99.9%	26.37 100.0%
Max./min. transmission	0.8776/0.7360	0.9729 and 0.7313	0.9413/0.8186
Data/restraints/parameters	8822/0/415	7055/0/361	7706/0/389
Goodness-of-fit on F^2	1.035	0.951	0.895
Final R indices [$I > 2\sigma(I)$]	$R_1 = 0.0568$, $wR_2 = 0.1752$	$R_1 = 0.0435$, $wR_2 = 0.1068$	$R_1 = 0.0608$, $wR_2 = 0.1404$
R indices (all data)	$R_1 = 0.0831$, $wR_2 = 0.2068$	$R_1 = 0.0710$, $wR_2 = 0.1145$	$R_1 = 0.1307$, $wR_2 = 0.1659$
Largest diff. peak and hole (e A^{-3})	0.637 and −0.527	0.354 and −0.343	0.505 and −0.625

The position of LMCT bands is found to shift to higher wavelengths (lower energy) when electron donating substituents are on the phenolate groups which would raise the energy of the frontier orbitals of the ligand and thus minimize the ligand-to-iron gap [7].

3.1. Description of crystal structure

The diffraction experiment and the structure refinement for the FeL^{NEC}, FeL^{NEB}, FeL^{NEM}, FeL^{NEBM}, FeL^{NEBu} and FeL^{NEOB} complexes

Table 4
Selected bond lengths (Å) and angles (deg) for compounds FeL^{NEC}, FeL^{NEB} and FeL^{NEM}.

FeL^{NEC}		FeL^{NEB}		FeL^{NEM}	
Bond lengths (Å)					
Fe1–O1	1.913(2)	Fe1–O1	1.901(3)	Fe1–O1	1.885(4)
Fe1–O2	1.895(2)	Fe1–O2	1.907(3)	Fe1–O2	1.902(3)
Fe1–O3	1.991(2)	Fe1–O3	1.992(4)	Fe1–O3	2.061(4)
Fe1–O4	2.028(2)	Fe1–O4	2.030(3)	Fe1–O4	2.007(4)
Fe1–N1	2.274(3)	Fe1–N1	2.235(4)	Fe1–N1	2.215(4)
Fe1–N2	2.232(3)	Fe1–N2	2.267(4)	Fe1–N2	2.268(4)
Bond angles (°)					
O2–Fe1–O1	96.54(10)	O1–Fe1–O2	96.06(14)	O1–Fe1–O2	96.99(15)
O3–Fe1–O4	86.17(9)	O3–Fe1–O4	86.03(14)	O4–Fe1–O3	84.88(15)
O1–Fe1–N1	85.11(9)	O1–Fe1–N1	85.88(14)	O1–Fe1–N1	87.43(16)
O1–Fe1–N2	92.98(10)	O1–Fe1–N2	165.75(15)	O1–Fe1–N2	166.55(16)
O3–Fe1–N1	91.51(10)	O3–Fe1–N1	168.56(14)	O3–Fe1–N1	86.54(16)
O3–Fe1–N2	168.75(10)	O3–Fe1–N2	90.84(15)	O3–Fe1–N2	86.33(15)
N2–Fe1–N1	79.58(10)	N1–Fe1–N2	79.88(15)	N1–Fe1–N2	79.26(16)

Table 5
Selected bond lengths (Å) and angles (deg) for compounds FeL^{NEBu}, FeL^{NEBM} and FeL^{NEOB}.

FeL^{NEBu}		FeL^{NEBM}		FeL^{NEOB}	
Bond lengths (Å)					
Fe1–O1	1.9349(18)	Fe1–O1	1.8802(14)	Fe1–O1	1.856(2)
Fe1–O2	1.878(2)	Fe1–O2	1.8716(14)	Fe1–O4	1.906(2)
Fe1–O3	1.977(2)	Fe1–O3	2.0022(14)	Fe1–O6	2.000(2)
Fe1–O4	2.063(2)	Fe1–O4	2.0753(15)	Fe1–O5	2.048(2)
Fe1–N1	2.300(2)	Fe1–N1	2.2420(17)	Fe1–N1	2.243(3)
Fe1–N2	2.203(2)	Fe1–N2	2.2400(17)	Fe1–N2	2.270(3)
Bond angles (°)					
O2–Fe1–O1	98.34(9)	O2–Fe1–O1	99.28(6)	O1–Fe1–O4	97.58(9)
O3–Fe1–O4	83.94(10)	O3–Fe1–O4	84.58(6)	O6–Fe1–O5	85.05(9)
O1–Fe1–N1	84.77(8)	O1–Fe1–N1	88.43(6)	O1–Fe1–N1	84.70(10)
O1–Fe1–N2	99.05(8)	O1–Fe1–N2	95.14(6)	O1–Fe1–N2	163.03(10)
O3–Fe1–N1	93.12(9)	O3–Fe1–N1	92.21(7)	O5–Fe1–N1	84.66(9)
O3–Fe1–N2	168.05(9)	O3–Fe1–N2	167.01(6)	O5–Fe1–N2	85.12(9)
N2–Fe1–N1	79.58(8)	N2–Fe1–N1	79.36(6)	N1–Fe1–N2	78.37(10)

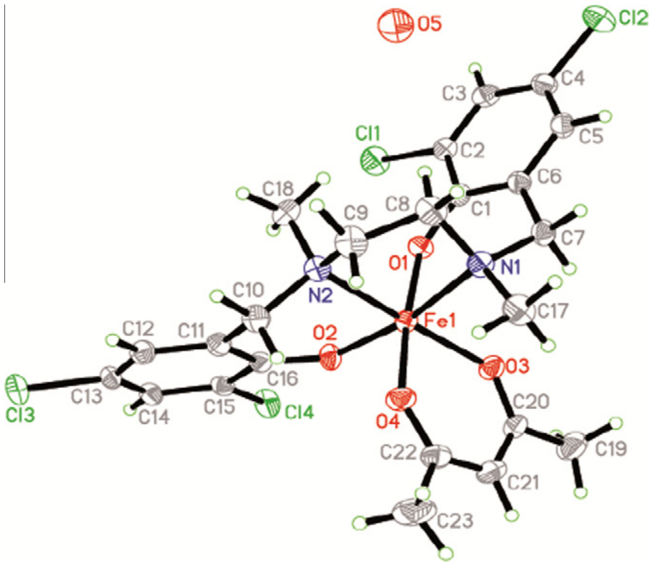

Fig. 2. ORTEP diagram and atom labeling scheme for complex FeL^{NEC} Ellipsoids are plotted at 30% probability level.

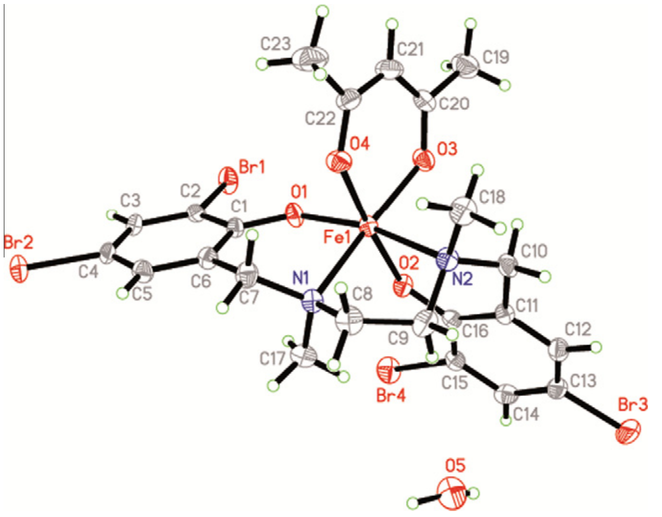

Fig. 3. ORTEP diagram and atom labeling scheme for complex FeL^{NEB} Ellipsoids are plotted at 30% probability level.

reported here are summarized in Tables 2 and 3. The selected bond lengths and angles are given in Tables 4 and 5.

In all structures reported here, the pairs of phenolic O atoms and the N atoms of the ligand occupy the *cis* positions within the Fe coordination sphere. Also the pair of acac oxygen atoms is bound in the *cis* arrangement. Consequently, the Fe ion has a FeN$_2$O$_4$ coordination sphere which has an octahedral geometry (Tables 4 and 5).

The overall molecular architecture of FeL^{NEC}, FeL^{NEB}, FeL^{NEM}, FeL^{NEBM} and FeL^{NEOB} complexes is similar. The tetradentate amine bis(phenolate) ligands form a curved part of the Fe environment, with the phenolic rings almost perpendicular to each other. The

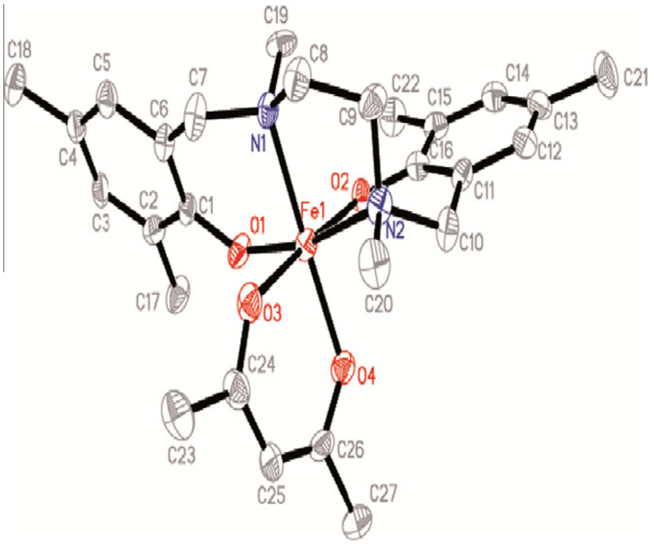

Fig. 4. ORTEP diagram and atom labeling scheme for complex FeL^{NEM} Ellipsoids are plotted at 30% probability level.

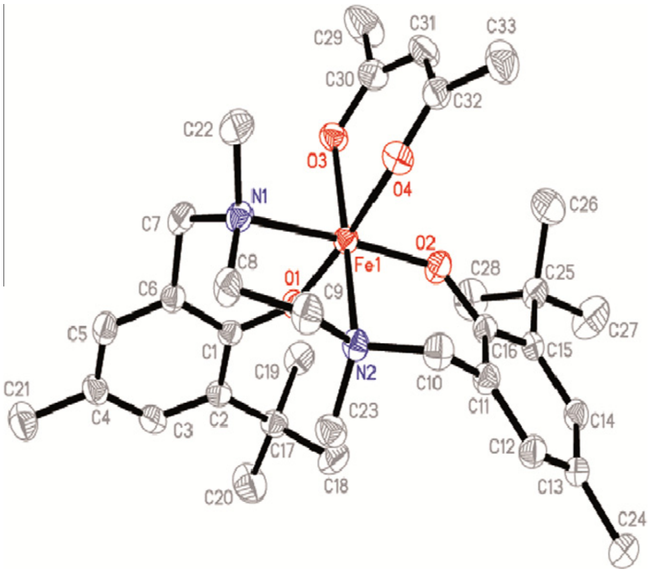

Fig. 5. ORTEP diagram and atom labeling scheme for complex FeL^{NEBM} Ellipsoids are plotted at 30% probability level.

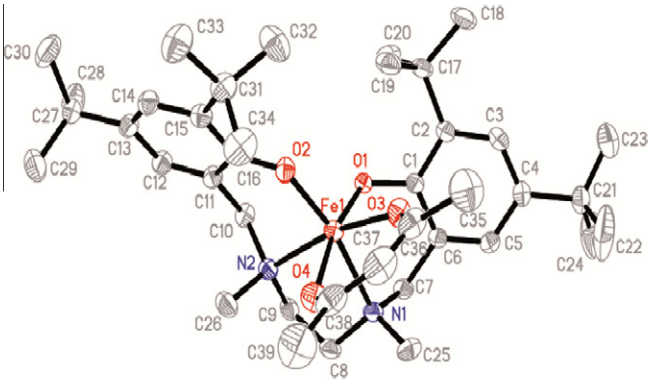

Fig. 6. ORTEP diagram and atom labeling scheme for complex FeL^{NEBu} Ellipsoids are plotted at 30% probability level.

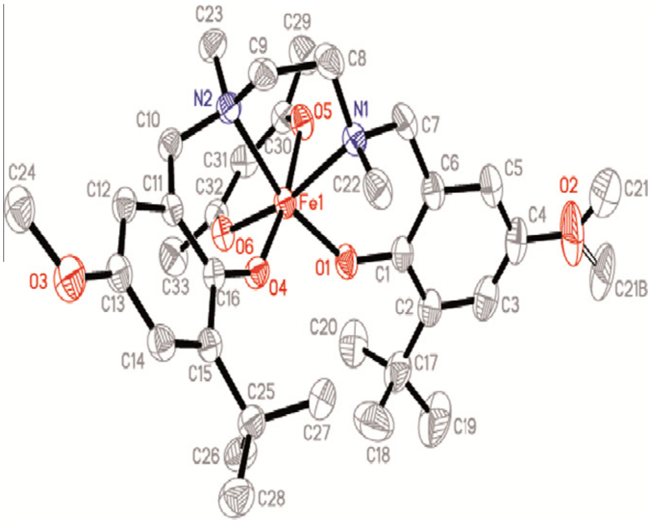

Fig. 7. ORTEP diagram and atom labeling scheme for complex FeL^{NEOB} Ellipsoids are plotted at 30% probability level.

acac ligands are bidentately coordinated to the central ion on the convex side of the amine bis(phenolate) ligands. The observed conformation of ethylenediamine moiety of the ligands is synclinal, with the N1–C8–C9–N2 torsion angle of −58.2(4)°, 56.5(6)°, −58.6(6)° and −59.7(2)° for FeL^{NEC}, FeL^{NEB}, FeL^{NEM}, FeL^{NEBM}, respectively. In FeL^{NEC}, FeL^{NEB} and FeL^{NEM} all substituents of the phenolic rings are co-planar with the rings, therefore not interfering with the position of acac ligands. The methyl groups bound to the ligand N atoms are positioned *trans* to each other, and are located on the opposite sides of the central Fe1–N1–C8–C9–N2 chelate ring. In such orientation, one of these N-Met moieties forms the weak intramolecular interactions with the acac ligands (Figs. 2–7). Such orientation has been found in Fe complexes of analogous ligands [25–27]. Only in FeL^{NEBu} complex, the N-Met groups are positioned *cis* to each other. In FeL^{NEBM}, FeL^{NEBu} and FeL^{NEOB} structures, the bulky tBu groups and the N-Met form a hydrophobic pocket, in which the acac ligand is accommodated. In all other complexes reported in this paper, the substituents are positioned co-planar with the phenolic rings and do not participate in the close interactions with the acac ligand.

3.1.1. X-ray crystal structure of FeL^{NEC} monohydrate

The asymmetric part of the reported structure consists of the Fe complex molecule containing L^{NEC} ligand forming four bonds to the central Fe(III) ion, the acac ligand and the water molecule, the last one has not bound to the central Fe ion (Fig. 2). The phenolate O1 and O2 of H_2L^{NEC} form the shortest bonds to the Fe(III), the distances being 1.913(2) and 1.895(2) Å, respectively, while the nitrogen atoms N1 and N2 form the longest bonds within the coordination sphere, the distances being 2.274(3) and 2.232(3) Å, respectively. The acac O3 and O4 participate in the Fe–O bonds of 1.991(2) and 2.028(2) Å, respectively. The largest deformation from the expected 90/180° values is found for O1–Fe1–N2 angle of 165.75(15)°.

Three chelate rings are formed by the L^{NEC} atoms and Fe ion. The Fe1–N1–C8–C9–N2 ring has a conformation twisted on C8–C9, while Fe1–O1–C1–C6–C7–N1 and Fe1–O2–C16–C11–C10–N2 rings have an envelope conformation. Also the chelate ring formed by the acac ligand has an envelope conformation.

The valence geometry of the L^{NEC} ligand is typical. The C–Cl distances vary from Cl1–C2 1.737(3) to Cl3–C13 1.748(3) Å. The O1–C1 and O2–C16 distances are 1.300(4) and 1.315(4) Å, respectively, and are similar to those found in other FeL^{NEX} complexes reported here. The N1–C8–C9–N2 torsion angle of −58.2(4)° reflects the strain caused by the tetradentate coordination of the ligand. The spatial orientation of two phenolic moieties is similar to that found for other complexes, with the dihedral angle between their planes being 74.6°. Position of the acac, as described with the dihedral angles between that plane and C1–C6 and C11−–C16 rings being 77.81° and 86.12°, respectively, is also similar to that found for the brominated analog in FeL^{NEB}.

There is a H-bond formed between the water molecule O5–H51A and the Cl2 atom, the O5···Cl2$[x-1,y,z]$ distance being 3.773 Å. Analysis of the crystal packing reveals the C–H···π interactions involving the N-Met group, with the distances to the centers of gravity C17–H17C···Cg(C11–C16) $[3/2-x,-1/2+y,1/2-z]$ of 2.89 Å and the intramolecular C17–H17A···Cg(O3–C20–C21–C22–O4–Fe1) of 2.62 Å, almost identical to those reported for FeL^{NEB}.

3.1.2. Crystal structure of FeL^{NEB} monohydrate

The asymmetric part of the reported structure consists of the Fe complex molecule containing L^{NEB} ligand forming four bonds to the central Fe(III) ion, the acac ligand and the water molecule, the last one has not bound to the central Fe ion (Fig. 3). The Fe ion has a FeN_2O_4 coordination sphere which has an octahedral geometry (Table 4). The phenolate O1 and O2 of L^{NEB} form the shortest bonds to the Fe(III), the distances being 1.901(3) and 1.907(3) Å, respectively, while the nitrogen atoms N1 and N2 form the longest bonds within the coordination sphere, the distances being 2.235(4) and 2.267(4) Å. The acac O3 and O4 coordinate to Fe1, with the Fe–O distances being 1.992(4) and 2.030(3) Å, respectively. The largest deformation from the expected 90/180° values is found for O1–Fe1–N2 angle of 165.75(15)°.

The chelate rings formed by the Fe ion and L^{NEB} and acac atoms have a conformation analogous to that described for FeL^{NEC} complex.

The valence geometry of the L^{NEB} ligand is typical. The C–Br distances vary from 1.889(5) to 1.905(5) Å. The O1–C1 and O2–C16 distances are 1.319(5) and 1.303(5) Å, respectively. The N1–C8–C9–N2 torsion angle is 56.5(6)°, reflecting the strain caused by the tetradentate coordination of the L^{NEB} ligand. The presence of the ethylenediamine bridge between two phenolic moieties results on the almost perpendicular orientation of the phenolic rings, with the dihedral angle between their planes being 73.2°. Also the plane of the acac ligand is almost perpendicular to the phenolic rings, the dihedral angles between that plane and C1–C6 and C11–C16 rings are 89.43° and 75.93°, respectively.

There is a H-bond formed between the water molecule O5–H51B and the Br atom, the O5···Br3$[x-1,y,z]$ distance being 3.813 Å. Analysis of the crystal packing reveals the C–H···π interactions involving the N-Met group, with the distances to the centers of gravity C18–H18A···Cg(C1–C6) $[1/2-x,1/2+y,1/2-z]$ of 2.85 Å and the intramolecular C18–H18C···Cg(O3–C20–C21–C22–O4–Fe1) of 2.68 Å.

3.1.3. X-ray crystal structure of FeL^{NEM}

The asymmetric part of the FeL^{NEM} structure consists of the Fe complex molecule containing L^{NEM} ligand, the acac ligand and the water molecule, the last one has not bound to the central Fe ion (Fig. 4).

Geometry of the FeN_2O_4 coordination sphere is octahedral (Table 4). The phenolate O1 and O2 of L^{NEM} form the shortest bonds to the Fe(III), the distances being 1.885(4) and 1.902(3) Å, respectively, while the nitrogen atoms N1 and N2 form the longest bonds within the coordination sphere, the distances being 2.215(4) and 2.268(4) Å. The acac O3 and O4 coordinate to Fe1, with the Fe–O distances being 2.061(4) and 2.007(4) Å, respectively. The largest deformation from the expected 90/180° values is found for O1–Fe1–N2 angle of 166.55(16)°.

Three chelate rings are formed by the L^{NEM} atoms and Fe ion. The Fe1–N1–C8–C9–N2 ring has a conformation twisted on C8–C9, while Fe1–O1–C1–C6–C7–N1 and Fe1–O2–C16–C11–C10–N2 rings have an envelope and twist boat conformation, respectively. Also the chelate ring formed by the acac ligand has an envelope conformation.

The valence geometry of the L^{NEM} ligand is typical. The O1–C1 and O2–C16 distances are 1.331(6) and 1.319(6) Å, respectively. The N1–C8–C9–N2 torsion angle is −58.6(6)°, reflecting the strain caused by the tetradentate coordination of the L^{NEM} ligand. Two phenolic moieties are almost perpendicular to each other, with the dihedral angle between the ring planes being 74.0°. Also the plane of the acac ligand is almost perpendicular to the phenolic rings, the dihedral angles between that plane and C1–C6 and C11–C16 rings are 89.43° and 75.93°, respectively.

There is a series of H-bonds involving the water O31 molecules, with the O31···O31 $[-x+1,-y,-z+1]$ distance of 2.410 Å. Analysis of the crystal packing reveals the intramolecular C–H···π interactions involving the N-Met group, with the distances to the centers of gravity C20–H20C···Cg(C1–C6) $[1/2-x,-1/2+y,1/2-z]$ of 2.80 Å.

3.1.4. X-ray crystal structure of FeL^{NEBM}

The asymmetric part of the reported structure consists of the Fe complex molecule containing L^{NEBM} ligand forming four bonds to the central Fe(III) ion and the acac ligand (Fig. 5). Within the coordination sphere, the pairs of phenolic O atoms and N atoms of the L^{NEBM} ligand, as well as acac oxygen atoms occupy the *cis* positions. The Fe ion has a FeN_2O_4 coordination sphere of an octahedral geometry (Table 5). Similar to other structures reported here, the phenolate O1 and O2 of L^{NEBM} form the shortest bonds to the Fe(III), the distances being 1.8802(14) and 1.8716(14) Å, respectively. The bonds formed by N1 and N2 nitrogen atoms are the longest, the distances being 2.2420(17) and 2.2400(17) Å, respectively. The acac O3 and O4 coordinate to Fe1, with the Fe–O distances being 2.0022(14) and 2.0753(15) Å, respectively. The largest deformation from the expected 90/180° values is found for O2–Fe1–N1 angle of 166.30(6)°.

Three chelate rings are formed by the L^{NEBM} atoms and Fe ion. The Fe1–N1–C8–C9–N2 ring has a conformation of an envelope on C9, the Fe1–O1–C1–C6–C7–N1 ring has a half-chair conformation, and Fe1–O2–C16–C11–C10–N2 ring has a screw-boat conformation. The chelate ring formed by the acac ligand has an envelope conformation.

The valence geometry of the L^{NEBM} ligand is typical. The O1–C1 and O2–C16 distances are 1.329(2) and 1.330(2) Å, respectively. The N1–C8–C9–N2 torsion angle is −59.7(2)°. The presence of the CNC_2NC bridge between two phenolic moieties results on the almost perpendicular orientation of the phenolic rings, with the dihedral angle between their planes being 84.5°. Also the plane of the acac ligand is almost perpendicular to the phenolic rings, the dihedral angles between that plane and C1–C6 and C11–C16 rings are 86.27° and 85.29°, respectively.

Analysis of the crystal packing reveals the C–H···π interactions involving the C1–C6 phenyl ring and tBu group C19–H19C···Cg(C1–C6)$[-x,1-y,-z]$ and C24 methyl group C24–H24C···Cg(C1–C6)$[1-x,1-y,-z]$. The respective distances between hydrogen atoms and the ring gravity center are 2.91 and 2.96 Å, respectively.

3.1.5. X-ray crystal structure of FeL^{NEBu}

The asymmetric part of the structure consists of the FeL^{NEBu} complex molecule. The L^{NEBu} ligand forms four bonds to the central Fe(III) ion (Fig. 6).

Architecture of the complex molecule is different from those found in FeL^{NEC}, FeL^{NEB} and FeL^{NEM} reported in this paper. In FeL^{NEBu} complex, the conformation of the N1–C8–C9–N2 bridge is −61.0(3)°, and both N-Met groups are positioned on the same side of the Fe–N1–C8–C9–N1 chelate ring, being cis to each other. In all other complexes reported here, these methyl groups are positioned on different sides of the corresponding ring. Such differences in the orientation of the analogous methyl groups have been reported before for similar complexes [25]. On the other hand, in complexes containing L^{NEBu} and monodentate axial Cl, Br or nitrate ligands, [26,27] the N-Met groups are positioned trans to each other as for FeL^{NEC}, FeL^{NEB} and FeL^{NEM} reported here.

The octahedral geometry of the Fe coordination sphere is similar to those found in other complexes reported here (Table 5). The phenolate O1 and O2 of L^{NEBu} form the shortest bonds to the Fe(III), the distances being 1.9349(18) and 1.878(2) Å, respectively, while the nitrogen atoms N1 and N2 form the longest bonds within the coordination sphere, the distances being 2.300(2) and 2.203(2) Å, respectively. The acac O3 and O4 participates in the Fe–O bonds of 1.977(2) and 2.063(2) Å, respectively. The largest deformation from the expected 90/180° values is found for O2–Fe1–N1 angle of 166.14(9)°.

The chelate rings formed by the Fe ion and L^{NEBu} and acac atoms have a conformation analogous to that described for FeL^{NEB} and FeL^{NEC} complexes. Only Fe1–O1–C1–C6–C7–N1 ring has a twist-boat conformation.

The valence geometry of the L^{NEBu} ligand is typical. The O1–C1 and O2–C16 distances are 1.350(3) and 1.335(3) Å, respectively, and are significantly longer than those found in complexes of chlorinated L^{NEC} or brominated L^{NEB} ligands. The N1–C8–C9–N2 torsion angle of −61.0(3)° and is similar to the values found for FeL^{NEB} and FeL^{NEC} complexes, although statistically significant differences values are observed.

The spatial orientation of two phenolic moieties is different from those found for other complexes, with the dihedral angle between their planes of 52.1°, being approximately 20° smaller than the values calculated for FeL^{NEB}, FeL^{NEC} and FeL^{NEM} complexes. The acac ligand is positioned in the narrow crevice between the N-Met and tBu moieties. The dihedral angles between the acac plane and C1–C6 and C11–C16 rings are 81.37° and 71.89°, respectively, is also similar to that found for complexes of the brominated and chlorinated ligands.

Analysis of the crystal packing reveals some hydrophobic intermolecular interactions. There is the C–H···π interaction involving the tBu C28–H28C group and the C11–C16[2−x,−y,1−z] ring, with the H···Cg distance of 2.73 Å.

3.1.6. X-ray crystal structure of FeL^{NEOB}

The asymmetric part of the reported structure consists of the Fe complex molecule containing L^{NEOB} ligand forming four bonds to the central Fe(III) ion and the acac ligand (Fig. 7). Within the coordination sphere, the pairs of phenolic O atoms and N atoms of the L^{NEOB} ligand, as well as acac oxygen atoms occupy the *cis* positions. The Fe ion has a FeN_2O_4 coordination sphere of an octahedral geometry (Table 5). Similar to other structures reported here, the phenolate O1 and O4 of L^{NEOB} form the shortest bonds to the Fe(III), the distances being 1.856(2) and 1.906(2) Å, respectively. Within the coordination sphere the bonds formed by N1 and N2 nitrogen atoms are the longest, the distances being 2.243(3) and 2.270(3) Å, respectively. The acac O5 and O6 coordinate to Fe1, with the Fe–O distances being 2.048(2) and 2.000(2) Å, respectively. The largest deformation from the expected 90/180° values is found for O1–Fe1–N2 angle of 163.03(10)°.

The chelate rings formed by the L^{NEOB} atoms and Fe ion have a following conformation: the Fe1–N1–C8–C9–N2 ring is twisted on C8–C9, while the Fe1–O1–C1–C6–C7–N1 and Fe1–O4–C16–C11–C10–N2 rings have an envelope conformation. The chelate ring formed by the acac ligand has a screw-boat conformation.

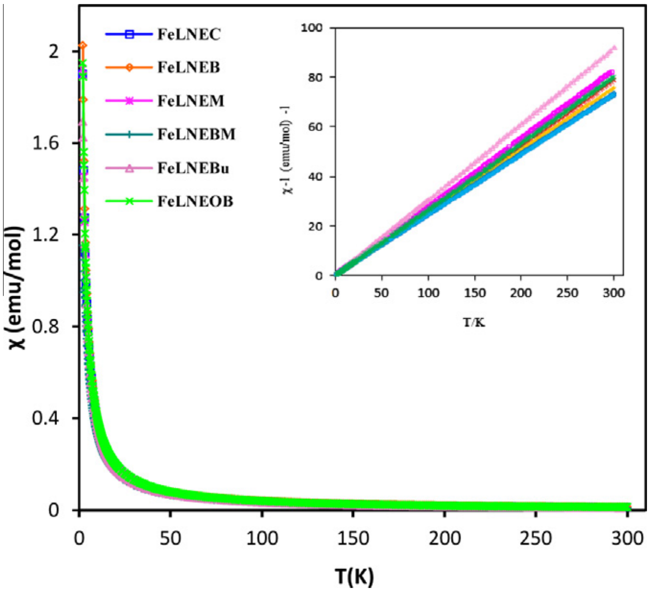

Fig. 8. Temperature dependent susceptibility $\chi(T)$ and inverse susceptibility $\chi^{-1}(T)$(inset) of FeL^{NEX} (X: C, B, M, BM, Bu and OB) measured in magnetic field of $H = 1000$ Oe.

The valence geometry of the L^{NEOB} ligand is typical. The O1–C1 and O2–C16 distances are 1.328(4) and 1.342(3) Å, respectively. The methoxy groups form the C4–O2 and C13–O3 bonds of 1.369(5) and 1.396(4) Å, respectively. The rotational disorder was detected for the O2–C21 methoxy group, with the occupancy of both alternative Met position estimated as 50% during the refinement. Both methoxy groups are co-planar with the phenolic rings, the torsion angles being C3–C4–O2–C21 178.5(10), C3–C4–O2–C21B −7.9(12) and C12–C13–O3–C24 5.2(5)°. The N1–C8–C9–N2 torsion angle is −58.7(4)°, and is similar to that found in all other structures reported here. The dihedral angle of 69.95° between two phenolic moieties is smallest for the series of the complexes reported here. Only in the FeL^{NEBu} complex with the flat architecture, that angle is significantly smaller, being 52.1°. Also the plane of the acac ligand is almost perpendicular to the phenolic rings, the dihedral angles between that plane and C1–C6 and C11–C16 rings are 81.57° and 89.30°, respectively.

The analysis of FeL^{NEOB} structure revealed an intramolecular interaction between C23 methyl and the gravity center of the chelate ring formed by acac ligand, the C23–H23A···Cg(Fe1–O5–O65) of 2.52 Å. Analysis of the crystal packing reveals the C23–H23C···O3[1/2−x,1/2+y,1/2−z] interaction with the C···O distance of 3.346 Å.

In the FeL^{NEOB} complex, the acac ligand is positioned between the C23 methyl bound to N1 and C20 methyl of the tBu group

Table 6
Calculated parameters *C* and θ from the fit of the measured data with Eq. (2). The effective magnetic moment μ_{eff} per iron ion was calculated using a relation $\mu_{eff} = \sqrt{8C}$ [28].

	C (emu K/mol)	θ (K)	μ_{eff} (BM)
FeL^{NEB}	4.1	−1.8	5.7
FeL^{NEM}	4.0	−1.5	5.7
FeL^{NEC}	3.7	3.3	5.4
FeL^{NEBu}	3.6	−0.6	5.4
FeL^{NEBM}	3.3	−0.9	5.1
FeL^{NEOB}	4.0	−0.1	5.7

Table 7
Electrode peak potentials for oxidation and reduction of complexes FeL^{NEX} (X: C, B, M, BM, Bu and OB).

	E_1^{ox}/V	E_2^{ox}/V	E_3^{ox}/V	E_4^{ox}/V	E_4^{red}/V	E_3^{red}/V	E_2^{red}/V	E_1^{red}/V
FeL^{NEC}	−1.06	-[*]	0.95	1.23	-	-	-	−1.15
FeL^{NEB}	−1.09	-	0.87	1.17	-	0.65	-	−1.23
FeL^{NEM}	-	-	0.68	1.04	-	0.60	−0.50	-
FeL^{NEBM}	−1.67	-	0.20	0.63	0.56	0.12	-	−1.77
FeL^{NEBu}	−1.3	−0.79	0.66	1.03	0.95	0.58	−0.85	−1.45
FeL^{NEOB}	−1.59	-	0.14	0.45	0.37	0.06	-	−1.67

[*] Redox behavior ill-defined.

bound to C2. Such arrangement is a consequence of the presence of bulky tBu group and N-Met near the Fe center, and is found also in FeL^{NEBu} and FeL^{NEBM}.

3.2. Magnetic susceptibility measurement

Magnetic susceptibility of powdered samples of FeL^{NEC}, FeL^{NEB}, FeL^{NEM}, FeL^{NEBM}, FeL^{NEBu} and FeL^{NEOB} were measured in a magnetic field of 1000 Oe as a function of temperature in the range 2–300 K with a Quantum Design MPMS-XL-5 magnetometer. The measured data were corrected for the sample holder contribution, for the temperature-independent Larmor diamagnetic susceptibility obtained from the Pascal's tables, and temperature independent paramagnetism [28].

Temperature variation of susceptibility $\chi(T)$ is shown in Fig. 8. The susceptibilities of all complexes increase with decreasing temperature and are practically the same for all investigated complexes. Only the inverse susceptibility graph $\chi^{-1}(T)$ shows small differences between the complexes.

As all inverse susceptibilities show linear temperature dependence, we applied a Curie–Weiss law in order to describe the measured data:

$$(= \mathrm{C}/(\mathrm{T} - {''}({''}) \tag{2}$$

The obtained parameters C and θ from the fit procedure with Eq. (2) and calculated effective magnetic moment μ_{eff} per iron ion are collected in Table 6.

The effective moments are between 5.4 and 5.7 Bohr magnetons (the magnetic moments recorded at 2–300 K). The values are close enough to the expected value for high spin Fe(III) of 5.9 BM [29] and thus confirming a high spin iron(III) in the structure.

The Curie–Weiss temperatures θ in Table 6 that are of the order of few Kelvins should be considered as additional fit parameters only, which slightly improve the fits rather than the indication of an antiferromagnetic or ferromagnetic coupling between the paramagnetic ion.

3.3. Electrochemistry

Cyclic voltammogram (CV) of complexes have been recorded in CH_2Cl_2 solutions containing 0.1 M $[(n\mathrm{Bu})_4\mathrm{N}]\mathrm{ClO}_4$ as a supporting electrolyte.

This research reveals that there are two oxidation peaks (E_3^{ox} and E_4^{ox}) for all complexes with a similar small difference in their redox potentials. Selected results are collected in Table 7. Typical cyclic voltammograms (CV) of FeL^{NEBu}, FeL^{NEBM} and FeL^{NEOB}, are presented in Figs. 9–12. The similarity of E_3^{ox} and E_4^{ox} values for all complexes in the range of 0.1–1.5 V suggests the same oxidation mechanism for all complexes.

These redox processes might be attributed to the ligand centered redox processes in which phenolate group yields phenoxyl radical in the complex, but there is no direct evidence available yet.

Comparison of the oxidation potentials of complexes suggesting that anodic oxidation processes are sensitive to the involved change in electron accepting of substituents on phenolate moieties of the ligands (Table 7).

On the other hand, the oxidation potentials of FeL^{NEX} (X: C, B, M, BM, Bu and OB), with electron accepting ligands are more positive than those for complexes with electron donating groups due to the

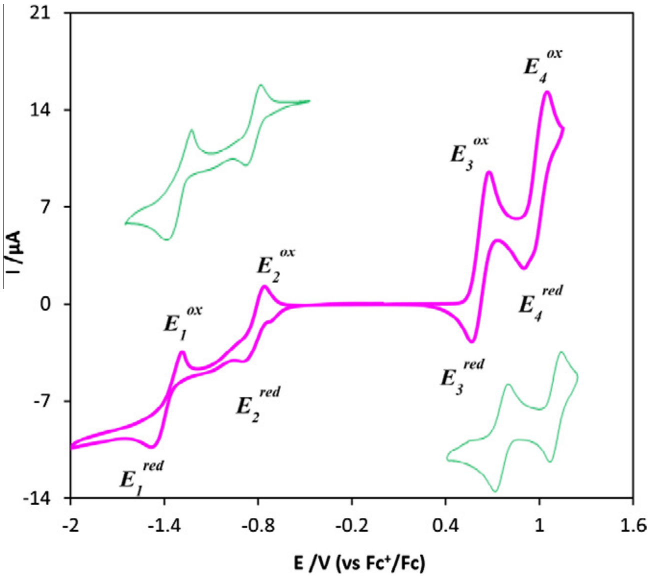

Fig. 9. Cyclic voltammogram of FeL^{NEBu} in CH_2Cl_2 at −70 °C (sc 20 mVs^{-1}) .

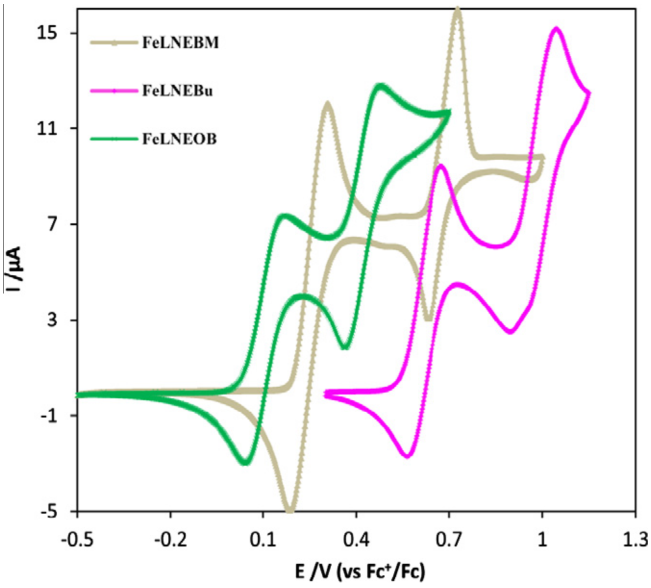

Fig. 10. Cyclic voltammograms of FeL^{NEBu}, FeL^{NEOB} and FeL^{NEBM} in CH_2Cl_2 at −70 °C (sc 20 mVs^{-1}).

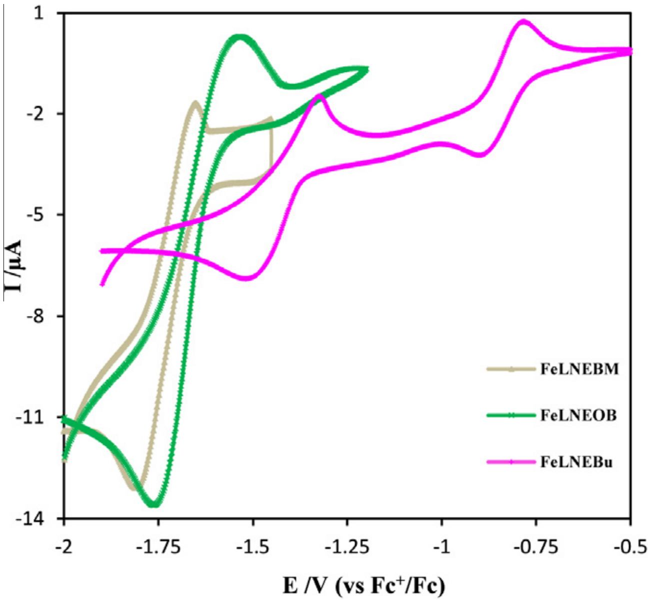

Fig. 11. Cyclic voltammograms of FeL^{NEBu}, FeL^{NEOB} and FeL^{NEBM} in CH_2Cl_2 at −70 °C (sc 20 mVs^{-1}).

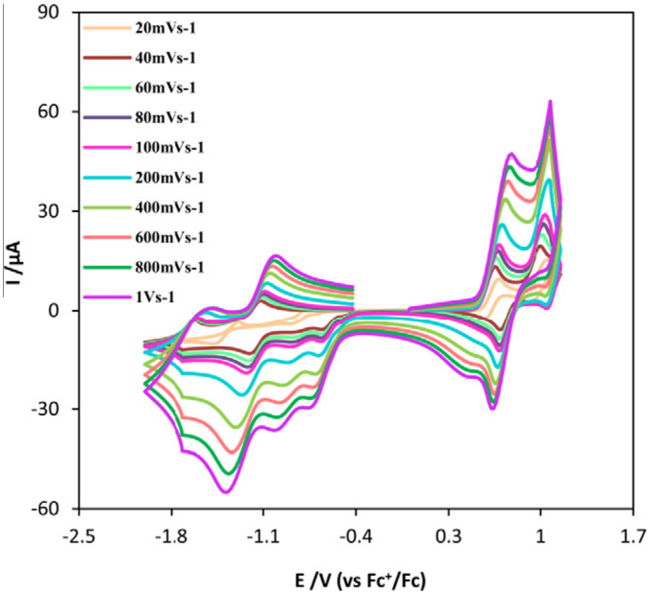

Fig. 12. Cyclic voltammograms of FeL^{NEBu} in CH_2Cl_2 at −70 °C (sc 20–1000 mVs^{-1}).

harder oxidation of phenolate ligands to the corresponding phenoxyl radical cations.

These ligand-centered voltammograms are electrochemically quasi-reversible, based on deviation of ΔE_p from 1 (ΔE_p is the separation of the oxidation and reduction peaks; the value of ΔE_p for reversible peaks is 1).

The metal-centered voltammograms have been observed in the negative potential range, what corresponds to the Fe^{III}/Fe^{II} reduction of iron complexes.

4. Conclusions

A series of iron complexes have been synthesized and characterized by IR, UV–Vis, elemental analysis and cyclic voltammetry techniques. Complexes FeL^{NEX} (X: C, B, M, BM, Bu and OB), have been structurally characterized by single crystal X-ray diffraction. X-ray structure analysis has revealed that all complexes are six coordinate and Fe(III) centers were surrounded by two phenolate oxygen atoms, two amine nitrogens and two oxygen atoms of acetylacetonate ligand similar to the proposed catechol-bound intermediate for catechol dioxygenase. In FeL^{NEBu} two of N-methyl groups occupy the *cis* position relative to each other, while in all other complexes reported here, the orientation is trans. Magnetic moment measurements confirm paramagnetic iron(III) in monomer complexes. All complexes undergo a metal-centered reduction and a ligand-centered oxidation. The oxidation potentials of complexes suggest that anodic oxidation processes are sensitive to the electron accepting properties of substituents on phenolate moieties of the aminophenol ligands.

Acknowledgments

Authors are grateful to the Institute for Advanced Studies in Basic Sciences (IASBS), Nicolaus Copernicus University and University of Ljubljana. E. Safaei gratefully acknowledges the support by the Institute for Advanced Studies in Basic Sciences (IASBS) Research Council under Grant No. G2012IASBS127.

Appendix A

The crystallographic data have been deposited with the Cambridge Crystallographic Data Centre, the CCDC numbers, 875144, 875145, 875146, 875147, 875148 and 875149 for FeL^{NEC}, FeL^{NEB}, FeL^{NEM}, FeL^{NEBu}, FeL^{NEBM} and FeL^{NEOB}, respectively.

These data can be obtained free of charge via http://www.ccdc.cam.ac.uk/conts/retrieving.html, or from the Cambridge Crystallographic Data Centre, 12 Union Road, Cambridge CB2 1EZ, UK; fax: (+44) 1223 336 033; or e-mail: deposit@ccdc.cam.ac.uk.

References

[1] T.D.H. Bugg, G. Lin, Chem. Commun. (2001) 941.
[2] L. Que, R.Y.N. Ho, Chem. Rev. 96 (1996) 2607.
[3] T. Funabiki, Oxygenases and model systems, in: R. Ugo, B.R. James (Eds.), Catalysis by Metal Complexes, vol. 19, Kluwer, Dordrecht, 1997. and Refs. therein.
[4] R.L. Crawford, D.L. Crawford, Enzyme Microb. Technol. 6 (1984) 434.
[5] F. Li, M. Wang, P. Li, T. Zhang, L. Sun, Inorg. Chem. 46 (2007) 9364.
[6] S. Harayama, M. Kok, E.L. Neidle, Annu. Rev. Microbial. 46 (1992) 565.
[7] R. Yamahara, S. Ogo, Y. Watanabe, T. Funabiki, K. Jitsukawa, H. Masuda, H. Einaga, Inorg. Chim. Acta 300–302 (2000) 587.
[8] Y. Hitomi, M. Yoshida, M. Higuchi, H. Minami, T. Tanaka, T. Funabiki, J. Inorg. Biochem. 99 (2005) 755.
[9] M. Merkel, M. Pascaly, B. Krebs, J. Astner, S.P. Foxon, S. Schindler, Inorg. Chem. 44 (2005) 7582.
[10] P. Mialane, L. Tchertanov, F. Banse, J. Sainton, J.-J. Girerd, Inorg. Chem. 39 (2000) 2440.
[11] M. Pascaly, M. Duda, F. Schweppe, K. Zurlinden, F.K. Muller, B. Krebs, J. Chem. Soc. Dalton Trans. 6 (2001) 828.
[12] M. Velusamy, R. Mayilmurugan, M. Palaniandavar, J. Inorg. Biochem. 99 (2005) 1032.
[13] R.B. Lauffer, R.H. Heistand, L. Que, Inorg. Chem. 22 (1983) 50.
[14] M. Merkel, F.K. Müller, B. Krebs, Inorg. Chim. Acta 337 (2002) 308.
[15] S. Ogo, R. Yamahara, T. Funabiki, H. Masuda, Y. Watanabe, Chem. Lett. 10 (2001) 1062.
[16] M.S. Shongwe, C.H. Kaschula, M.S. Adsetts, E.W. Ainscough, A.M. Brodie, M.J. Morris, Inorg. Chem. 44 (2005) 3070.
[17] M. Velusamy, R. Mayilmurugan, M. Palaniandavar, Inorg. Chem. 43 (2004) 6284.
[18] M. Velusamy, M. Palaniandavar, R.S. Gopalan, G.U. Kulkarni, Inorg. Chem. 42 (2003) 8283.
[19] R. Viswanathan, M. Palaniandavar, T. Balasubramanian, T.P. Muthiah, Inorg. Chem. 37 (1998) 2943.
[20] Y. Zang, J. Kim, Y. Dong, E.C. Wilkinson, E.H. Appelman, L. Que, J. Am. Chem. Soc. 119 (1997) 4197.
[21] G.M. Sheldrick, SHELXS97 and SHELXL97, University of Gőttingen, Germany, 1997.
[22] CrysAlis CCD171 and RED171 package of programs, Oxford Diffraction, 2000.
[23] E. Safaei, I. Saberikia, A. Wojtczak, Z. Jagličić, A. Kozakiewicz, Polyhedron 30 (2011) 1143.

[24] E. Safaei, H. Sheykhi, A. Wojtczak, Z. Jagličić, A. Kozakiewicz, Polyhedron 30 (2011) 1219.
[25] P. Mialane, E. Anxolabéhère-Mallart, G. Blondin, A. Nivorojkine, J. Guilhem, L. Tchertanova, M. Cesario, N. Ravi, E. Bominaar, J.-J. Girerd, E. Münck, Inorg. Chim. Acta 263 (1997) 367.
[26] J.B.H. Strautmann, S.D. George, E. Bothe, E. Bill, T. Weyhermùller, A. Stammler, H. Bögge, T. Glaser, Inorg. Chem. 47 (2008) 6804.
[27] K. Hasan, C. Fowler, P. Kwong, A.K. Crane, J.L. Collins, Ch.M. Kozak, Dalton Trans. (2008) 2991.
[28] O. Kahn, Molecular Magnetism, VCH Publishing, 1993.
[29] N.W. Ashcroft, N.D. Mermin, Solid State Physics, Saunders College Publishing, USA, 1976.